Addressing Resiliency of In-Memory Floating Point Computation

Sina Sayyah Ensan, Swaroop Ghosh, Seyedhamidreza Motaman, and Derek Weast

School of Electrical Engineering and Computer Science, Pennsylvania State University, University Park, PA 16802 USA

(sxs2541, szg212, sxm884, dqw5347)@psu.edu

Abstract—**In-memory computing (IMC) can eliminate the data movement between processor and memory which is a barrier to the energy-efficiency and performance in Von-Neumann computing. Resistive RAM (RRAM) is one of the promising devices for IMC applications (e.g. integer and Floating Point (FP) operations and random logic implementation) due to low power consumption, fast operation and small footprint in crossbar architecture. In this paper, we propose FAME, a pipelined FP arithmetic (*adder/subtractor*) using RRAM crossbar based IMC. A novel shift circuitry is proposed to lower the shift overhead during FP operations. Since 96% of the RRAMs used in our architecture are in High Resistance State (HRS), we propose two approaches namely Shift-At-The-Output (SATO) and Force To V_{DD} (FTV) (ground (FTG)) to mitigate Stuck-at-1 (SA1) failures. In both techniques, the fault-free RRAMs are exploited to perform the computation by using an extra clock cycle. Although performance degrades by 50%, SATO can handle 50% of the faults whereas FTV can handle 99% of the faults in the RRAM-based compute array at low power and area overhead. Simulation results show that the proposed single precision FP adder consumes 335 pJ and 322 pJ for $NAND$-$NAND$ and NOR-NOR based implementations, respectively. The area overheads of SATO and FTV are 28.5% and 9.5%, respectively.**

Index Terms—**In-Memory Computing, Floating Point, RRAM, Crossbar, Resiliency.**

I. INTRODUCTION

In the big data era, conventional CMOS-based Von-Neumann architecture platforms are unable to face real-time data processing requirements [1]. Memory and computing elements are decoupled from each other in Von-Neumann architecture [2] which apply frequent communication between memory and computing cores [3]. The compute energy has been scaled asymmetrically compared to data transport energy with transistor scaling. Data movement in modern computing systems dominates energy-efficiency and performance [4].

In Memory Computing (IMC) is one of the promising compute models to fully or partially eliminate the need to transport data between processors and memory. The main concept of IMC is to infuse compute capability into the memory cells [5]. IMC is achievable by using emerging Non-Volatile Memories (NVM) e.g., RRAM, Spin Transfer Torque (STT) RAM and Phase Change Memory (PCM) [5], [6], [7], [8]. Near memory processing [9] and logic-in-memory, which employ NVMs in the logic space [10], [11] to preserve states between powering sequence have been proposed in the literature. However, they cannot solve the problem of separation between logic and memory.

IMC modifies memory cells and/or peripheral circuits/access mechanisms to infuse compute capability into memory cells. IMC can solve specific tasks such as, dot-products for recognition [8], search [12] and classification [6]. It also supports a wide range of logic and arithmetic operations [10], [13], [14], [15]. NVM-based IMC using STTRAM [16], RRAM [17], Ferroelectric FET (FeFET) and Phase-Change Memory [18] are becoming popular.

Due to immature fabrication technology limitations, manufacturing yield is still a serious concern for NVMs such as, RRAM crossbar. Faults in RRAM crossbar arrays are categorized into hard and soft faults [1]. Previous studies have been predominantly focused on soft faults [19] whereas few attempts are made to recover crossbar arrays from hard faults. The soft faults (e.g., read disturb) can be recovered by calibrating the resistance [19] [20]. However, hard faults are recovered through mapping algorithms (i.e., by assigning inputs of faulty RRAMs to the redundant rows or columns) [1], [21], [22].

Stuck-at fault is defined as a situation when the RRAM is permanently stuck at High Resistance State (HRS) or Low Resistance State (LRS). It has been reported [23] that only 63% of HfO_2- based RRAM devices for 4Mb crossbar array are fault-free and about 10% of RRAM devices contain stuck-at faults. Retention failure which is similar to the resistive switching due to the generation or recovery of oxygen vacancy is another type of hard faults in RRAMs. In the proposed IMC architecture, only 4% of the RRAMs are in LRS and the other 96% are in HRS. Therefore in this paper, we focused on the HRS retention failure and stuck-at-1 (i.e., stuck-at HRS) faults. If the yield of a single RRAM device is 99%, there is only 10^{-9} probability for a column of 64*32 array to be fault free. The stuck-at failures and HRS to LRS switching [24] can be fixed by employing few redundant rows/columns when RRAM array is considered working as a memory. However, the whole array is needed for IMC application. Consequently, computations will fail due to errors in the absence of fault tolerance schemes.

We have considered Floating Point (FP) operations to evaluate the proposed resilience techniques. This is motivated by the fact that emerging applications e.g., mission-critical systems like autonomous cars require huge amount of data processing in real-time at low-power (to make timely decisions). The autonomous cars make complex decisions in a tight deadline using algorithms e.g., Kalman filters for data

fusion, ray tracing for path planning and, edge detection and deep neural networks for classification. Most of these algorithms require FP vector operations involving transpose, inverse, addition/multiplication. Therefore, the capability to perform these tasks, quickly and accurately can be of utmost importance to enable the safe and energy-efficient autonomous systems. Conventionally, FP architectures are implemented as full custom VLSI or in FPGA. Although fast and power efficient, these custom designs impose cost and complexity. In this paper, we propose FAME (Single Precision Floating Point Arithmetic using In-Memory Computing) implemented on crossbar RRAM. We employ a modified version (Section **??**) of Dynamic Computing In Memory (DCIM) [7] based architecture as our baseline compute substrate for FAME. Additionally, two approaches namely, Shift-At-The-Output (SATO) and Force To $V_{DD}(GND)$ (FTV(G)) are proposed to enable in-memory computing in presence of HRS to LRS retention failures. We focus on this failure mechanism due to two reasons: (i) HRS to LRS switching is more common in RRAM [25]; (ii) majority of the RRAMs (96%) are in HRS for both $NAND$-$NAND$ and NOR-NOR arrays. Carry Select Adder (CSA) based on DCIM implementation is used for the demonstration. We add extra peripheral circuits on each array to implement the proposed techniques.

In particular, we make the following contributions in this paper:

1) Alternative low-overhead realization of DCIM for FP computation;
2) In-memory shift circuit embedded in the peripherals e.g., sense amplifier (SA);
3) Enabling pipeline architecture using the latch embedded in the SA;
4) Propose fault mitigation approaches such as, SATO and FTV/FTG for DCIM architecture;
5) Conduct PV analysis of the RRAM array to check the integrity of SATO and FTV/FTG.

Rest of the paper is organized as follows. Section II introduces related work on IMC. Section **??** explains the proposed FAME circuit and architecture. Section III presents the simulation results of FAME and comparison with other IMC logic implementation. Section IV explains proposed approaches to overcome SA1 faults in IMC architecture. Section V presents the proposed fault tolerance approaches and simulation results. Section VI draws the conclusion.

II. RELATED WORK AND BACKGROUND

A. Memristor Aided Logic (MAGIC)

MAGIC [26] (shown in Fig. 1) is an IMC architecture in which logic state of the gates are represented by the memristor (RRAM in this paper) resistance where high (low) resistance is considered as logic '1' ('0'). The inputs to a MAGIC gate are the logic states stored in the input memristors and the output is the final state of the output memristor. MAGIC executes operations in two steps: 1) setting the output memristor to a known logic state (e.g., for NOR operation the output
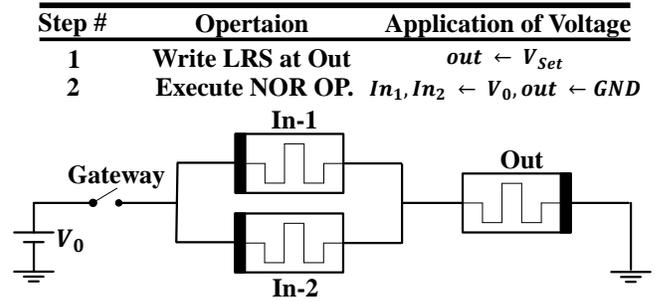
Step #	Opertaion	Application of Voltage
1	Write LRS at Out	$out \leftarrow V_{Set}$
2	Execute NOR OP.	$In_1, In_2 \leftarrow V_0, out \leftarrow GND$

Fig. 1: MAGIC NOR

is in LRS); 2) applying a known voltage (V_0) to the input memristors which causes current flow through the input and output memristors. The output memristor's state changes if the current passing through it is higher than the set/reset current. MAGIC is capable of implementing Boolean functions such as, $NAND$, NOR, AND, OR and NOT.

B. Dynamic Computing In Memory (DCIM)

DCIM [7] is an RRAM crossbar based architecture, which each memory cell is composed of an RRAM device connected in series with a selector diode (Fig. 2a. In-memory computation is accomplished by implementing the functions in the form of Sum-of-Product (SoP). Thus, both AND and OR operations are required to implement the logical functions.

In DCIM, wordlines (WL) serve as the inputs and the bitlines (BL) serve as the outputs of the arrays. Separate pre-programmed AND and OR arrays are dedicated to implement the desired function. For instance, in order to implement $in_0.\overline{in_1}$, the bitcells connected to in_0 and $\overline{in_1}$ are programmed to LRS while the bitcells connected to $\overline{in_0}$ and in_1 are programmed to HRS (Fig. 2a. All bitcells which are not part of AND gate inputs are programmed to HRS (e.g., the bitcells connected to input in_n and $\overline{in_n}$).

Fig. 2 shows the implementation of XOR function using DCIM. Initially, Pre signal is activated to pre-charge BLs of the AND array. Next, inputs (in_0 and in_1) are applied by asserting EN_{AND}. As shown in Fig. 2b, both BL_0 and BL_1 drop below the reference voltage ($V_{Ref-AND}$) when $in_0 = in_1 = 1$. As a result, SA output which determines the results of $in_0.\overline{in_1}$ and $\overline{in_0}.in_1$ functions are pulled down to '0' at the edge of SE_{AND}. Next, AND array SA outputs are provided as inputs to the OR array. Since inputs of the OR array are '0', the BL ($BL0_{OR}$) remains discharged which results in $in_0 \oplus in_1 = 0$. If $in_0 = 0, in_1 = 1$ ($in_0.\overline{in_1} = 0$ and $\overline{in_0}.in_1 = 1$), BL_0 discharges while BL_1 remains pre-charged. Therefore, $BL0_{OR}$ starts charging at the edge of EN_{OR}. Finally, the voltage of $BL0_{OR}$ is compared against V_{Ref-OR} at the edge of SE_{OR} which produces '1' at the output of SA.

C. FP Addition/Subtraction

In IEEE 754 standard, a single precision FP number is represented by 1 Sign bit, 8 Exponent bits, and 23 Fraction bits. A negative (positive) number is represented with a sign bit
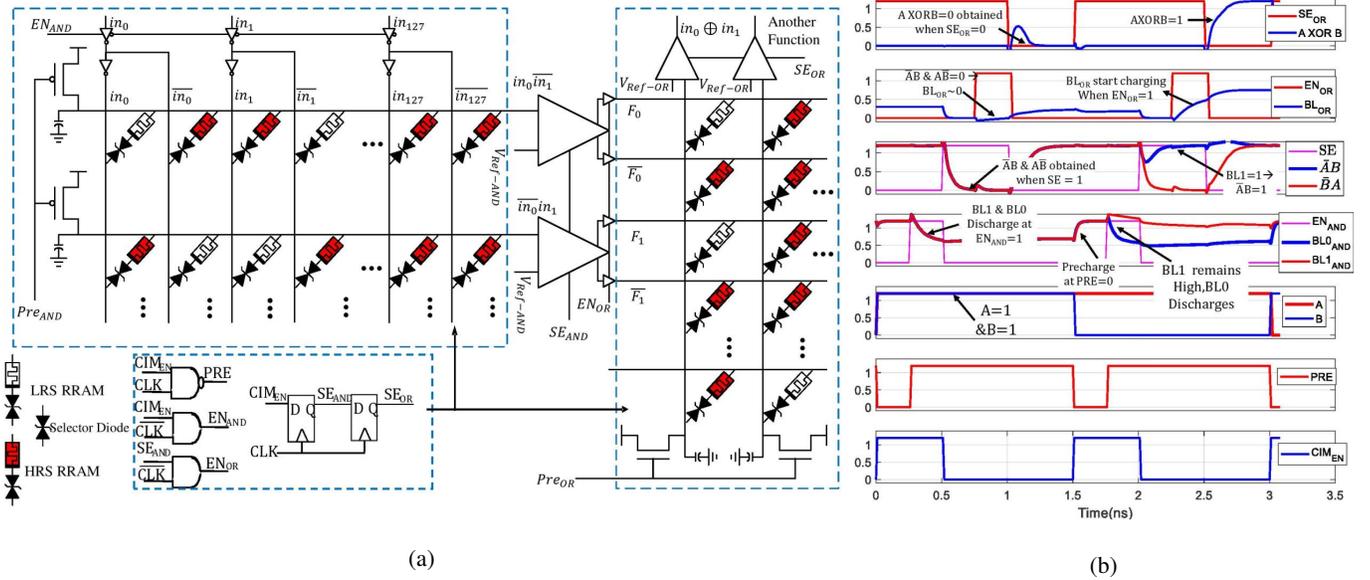
Fig. 2: (a) XOR implementation using DCIM architecture in RRAM crossbar array; and, (b) timing diagram of logical XOR operation.
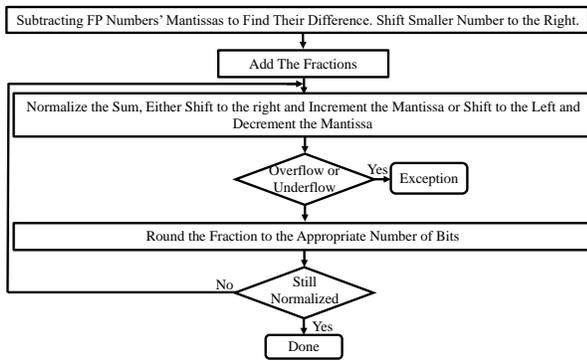

Fig. 3: IEEE 754 Standard FP addition/subtraction Flowchart [27]

TABLE I: Simulation parameters

Parameter	Value
MOSFET Gate Length	65 nm
NMOS/PMOS Threshold Voltage	423/-365 mV
BL Capacitance	30 fF
RRAM Gap Min/Max/Oxide Thickness	0.1/1.7/5 nm
Atomic Energy for Vacancy Generation/Recombination	1.501/1.5 eV
RRAM Write Latency	25 ns
RRAM HRS/LRS at 1.2V	6.68 M/58.9 K Ω

TABLE II: Monte Carlo simulation parameters

Parameter	Real Value	Variation	STD. Deviation
RRAM LRS Gap	0.1 nm	7%	3σ
RRAM HRS Gap	1.7 nm	7%	3σ
MOS Oxide Thickness	1.2 nm	10%	3σ
MOS Gate Length	65nm	10%	3σ

equal to '1'('0'). In order to demonstrate negative exponents, IEEE 754 uses a bias of 127 for single precision (e.g., -1 is represented by -1+127=126). The general representation of a FP number is given by:

$$(-1)^{Sign} * (1 + Fraction) * 2^{(Exponent-Bias)} \quad (1)$$

The flowchart for FP addition/subtraction as per IEEE 754 standard is shown in Fig. 3.

III. FAME SIMULATION RESULTS

The simulations are carried out in 65nm PTM [28] technology by employing ASU RRAM model [29] and bi-directional selector diode model [30]. Worst-case Sense Margin (SM), BL-delay, average delay, average power, and energy consumption (Table III) are calculated to evaluate FAME architecture. Key parameters of devices for simulations are listed in Table I. SM is obtained by performing 1000 point Monte Carlo simulations at various temperatures with parameters listed in Table II to mimic process variations.

The worst-case SM is obtained under process variation @25°C for worst case compute array (i.e., fraction addition array). The BL-delay is the time when 100 mV SM is achieved. The proposed FP adder/subtractor implementation with both $NAND$-$NAND$ and NOR-NOR architecture are compared against MAGIC and ASIC design.

The write latency is obtained by performing 1000 points MC simulation. The worst-case write latency for low-to-high and high-to-low switching under process variation is 20ns. FAME achieves 828X, 3.2X and 3.7X improvement in latency, power and energy, respectively compared to MAGIC. The higher energy associated with MAGIC is attributed to the need to write into the RRAMs when an operation is done. Furthermore, compared to the power, energy consumption, and

TABLE III: Simulation results

Characteristics	$NAND$	NOR	MAGIC	CPU [32]
BL Delay (ns)	1.42	1.23	N/A	N/A
SA Sense Delay (ps)	24.52	69.1	N/A	N/A
Average Delay	25ns	23ns	20us	84ns
Exp. Subt. Pow. (uW)	443.31	448	2808.92	N/A
Fr. Add. Pow. (uW)	1068.52	1123.19	2142.84	N/A
Shift Pow. (uW)	443.24	452.93	982.31	N/A
Avg. Power (mW)	0.7	0.71	2.3	61
Energy (nJ)	0.33	0.32	1.2	5.1

TABLE IV: SM in different temperatures

SM (mv) / Temp	$-10°$	$25°$	$90°$
$NAND$	94.5499	91.30245	79.26
NOR	105.6009	104.3965	99.7171

delay imposed by transferring data between main memory and processing units (e.g. CPU, GPU, and FPGA), FAME reduces power and energy consumption and delay by 98.8%, 93.7%, and 70.2%, respectively.

A 1000 point MC simulations are performed at -10°C, 25°C, and 90°C at $1.2V$ supply voltage to obtain mean of SM (Table III). V_{NAND0} (NAND array BL voltage when input is '0'), V_{NAND1}, V_{NOR0}, and V_{NOR1} distributions at worst-case temperature are shown in Fig. 4. In order to achieve the read access pass yield ($RAPY$) [31] [7] we have performed SA offset voltage analysis. The SA offset voltage can be modeled by a Gaussian distribution with $\sigma = 16mV$ and $\mu = 8mV$. To obtain $RAPY$ we assume that V_{Ref} is produced by a voltage regulator with negligible variation ($5mV$). We assigned V_{Ref} in such a way to maximize $RAPY$. Based on the Monte-Carlo simulation, the RAPY of $NAND$ and NOR operations are found to be 4.6σ and 4.5σ respectively.

IV. RESILIENCE TO STUCK-AT FAULT

In this section, we describe SATO and FTV, two fault mitigation techniques proposed for DCIM architecture. In the following we use, (i) faulty BL to denote each BL with an

TABLE V: FAME area

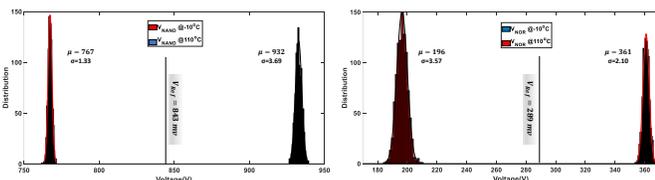| Block	Array Size	# of Arrays
Exponent Subtraction 1st $NAND$	32*32	1
Exponent Subtraction 2nd $NAND$	32*64	1
Right Shift	8*16	1
Fraction Addition 1st $NAND$	64*64	2
Fraction Addition 2nd $NAND$	64*64	2
Left Shift	32*64	1
Exponent Inc/Dec 1st $NAND$	32*32	1
Exponent Inc/Dec 1st $NAND$	32*64	1

Fig. 4: SM distribution.

undesired stuck-at-1 (SA1) RRAM; (ii) faulty WL (BL) to denote each WL (BL) with an undesired SA1 RRAM.

Computations are performed in two cycles when the proposed fault mitigation techniques are applied (Fig. 5). The computations of fault-free BLs (BL_1, BL_2 and BL_3 in Fig. 5 (a)) are performed in the first cycle and the computations of the faulty BLs (BL_0 in Fig. 5 (a)) are performed in the second cycle. In FTV, the WLs corresponding to faulty RRAMs ($\overline{In_2}$ in Fig. 5 (a)) for $NAND$ (AND) array are forced to V_{DD} to mask faulty bits. In a dual Force-to-Ground (FTG) technique, the faulty BLs are forced to 0V for NOR (OR) arrays. FTV/FTG tolerates 99% of stuck-at faults (SAF) while reducing power consumption of the array. In SATO approach, operations of fault-free BLs are executed in the first cycle and then the outputs are shifted in the SAs. Then, the operations of faulty BLs are computed using fault-free BLs (operation of BL_0 is done in BL_1). SATO covers 50% of SAFs without affecting power consumption. The high level timings of FTV and SATO are illustrated in Fig. 5 (b) and (c), respectively.

A. Shifting-At-The-Output (SATO)

As described before, in this technique the normal operation for fault-free BLs are performed in the first cycle and computation of faulty BLs are performed in the second cycle. SATO does not use faulty BLs for performing an operation and executes all the operations on the fault-free BLs. SATO shifts the data stored in SAs' latch of fault-free BLs to prevent overwriting. When computation of first cycle is completed, the data are shifted in SAs (three shifts are needed if an adder/subtractor is implemented). As shown in Fig. 6, inputs of the WLs should get shifted too, so computation is performed using fault-free BLs. Peripherals of SATO incurs 29.5% area overhead.

1) Non-fixable Faults: SATO cannot handle faults that appear on two consecutive sets of BLs (each three consecutive BLs are a set if an adder/subtractor is implemented). More multiplexers are needed for each WL to handle faults on consecutive sets of BLs. The number of multiplexers per WL increases linearly with the number of consecutive faulty sets of BLs to be handled by SATO. For example, if faults occur on two consecutive sets of BLs (e.g., if BL_3 in Fig. 6 also contains a fault) SATO cannot handle it unless two or more multiplexers are dedicated to each WL. The probability of two faults occurring on two consecutive BL is less than 3% for a 64*32 crossbar array. However, SATO is able to handle less than 50% of the faults if a yield of 99.5% is considered on a crossbar array.

2) Handling multiple faults: SATO's efficiency degrades for increasing number of faults. In this paper, we considered a yield of 99.5% in a 64*32 crossbar array for SATO simulations. This corresponds to 11 randomly distributed faults throughout the array. SATO is able to mitigate around 50% of the faults in the array. Faults have been distributed on the memory cells using $rand$ function provided by $C++$ programming language.
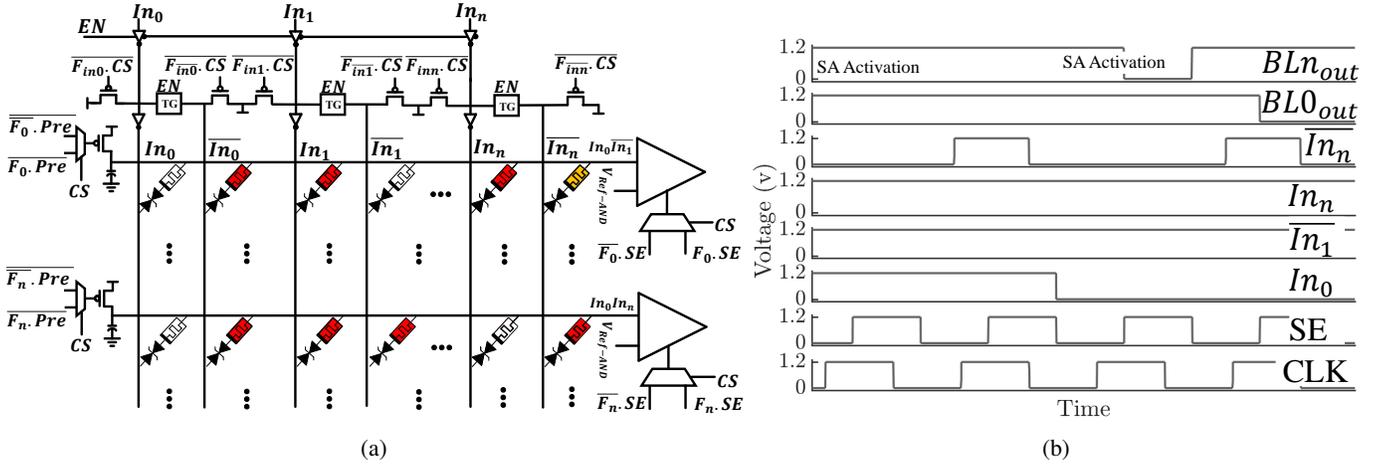
(a)

(b)

Fig. 7: FTV: (a) fault mitigation in undesired LRS RRAMs; (b) timing diagram.
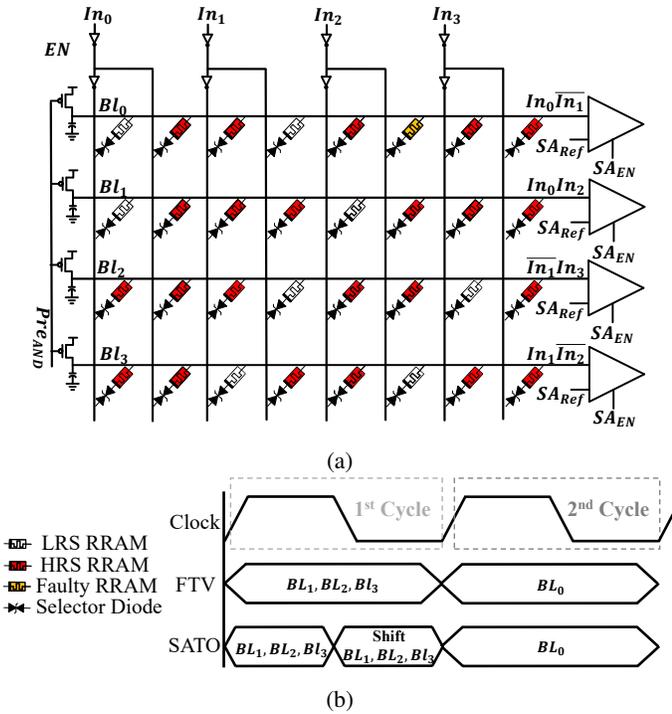

(a)

(b)

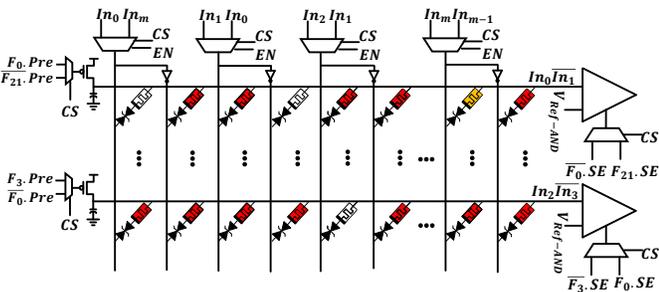Fig. 5: (a) 4*4 RRAM crossbar array, (b) FTV and SATO timing.

Fig. 6: SATO fault mitigation technique.

B. Forcing to V_{DD} (FTV)

FTV performs operations of fault-free and faulty BLs in the first and second cycle, respectively. Inputs of faulty RRAMs are forced to V_{DD} in the second cycle. To apply FTV to $NAND$ arrays, we follow a simple $NAND$ logic where for example $A \cdot B \cdot C$ is replaced with $A \cdot B \cdot 1$, where C is the input of the SA1 RRAM. Therefore, $NAND - 2$ is performed in $NAND - 3$ form with an extra '1' which do not affect the logic. However, increased number of RRAMs in a BL reduces the SM. If the faults are located on different BLs, they do not affect the SM.

FTV uses a multiplexer for the enable signal of SAs to ensure that the array is capable of working in two cycles. $\overline{F} \cdot \overline{CS}$ and $F \cdot CS$ are inputs of the multiplexer, where F is '0' if the BL is fault-free and is '1' if the BL is faulty. CS is the clock sequence initialized to '0' in the first cycle and '1' in the second cycle. Enable signal of SAs connected to fault-free BLs are asserted in the first cycle while the enable signal of SAs connected to faulty BLs is asserted in the second cycle to save power and maintain the correct logic. Furthermore, FTV uses 4 additional transistors compared to DCIM at the WL input to enable the test procedure (explained in Section IV-C) to find faulty RRAMs.

As shown in Fig. 7a, FTV uses two transmission gates to connect $input$ and $\overline{input}$ to WLs. Also, one PMOS transistor is added to each WL to force the WL to V_{DD} when is needed in the second cycle. In the second cycle, SC signal of faulty WLs gets activated to force faulty WLs to V_{DD}. FTV employs a fault signal (F_W) for each WL to track the faulty WLs and set them to V_{DD} in the second cycle. FTV also defines a fault signal (F_B) for each BL to keep track of faulty BLs. Additional circuitry and peripherals needed to apply FTV to the DCIM increase the area by 9.5%.

1) Forcing-to-Ground (FTG): The basic concept of FTG is similar to FTV but it applies to NOR (OR) arrays. FTG follows simple logic that number of '0's is not important in NOR (OR) operation. Therefore, FTG forces inputs of faulty
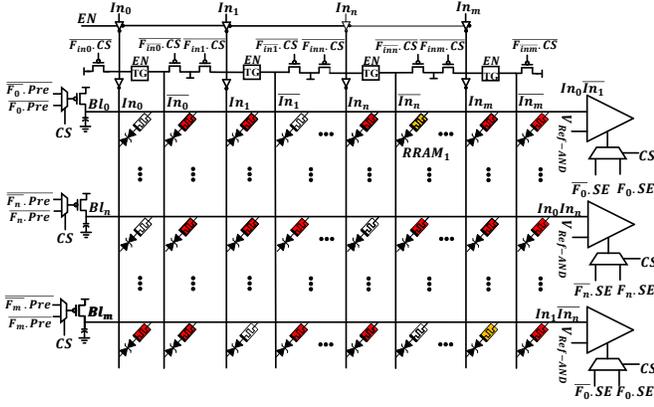
Fig. 8: Faults that cannot be handled by FTV.

TABLE VI: Comparison between SATO and FTV

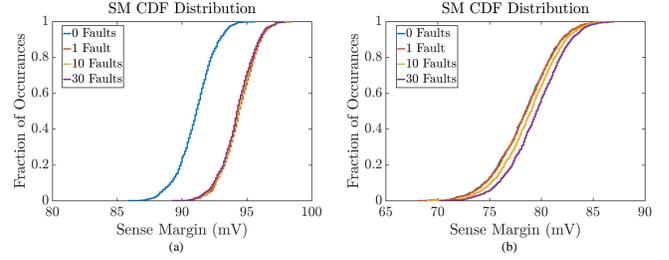| Characteristics	SATO	FTV
Coverage	50%	90%
SM (w/ diode)	Not Affected	Not Affected
SM (w/o diode)	Not Affected	Lower
Test circuitry	Needed	Included
Area overhead	28.5%	9.5%
Power	Not affected	Lower
Energy	Higher	Slightly Lower
Performance	50%	50%

Fig. 9: Process variation analysis of SM for various number of failures on a single BL with selector diode in the bitcell i.e., selector diode-RRAM crossbar at, (a) $-10°C$; (b) $90°C$.
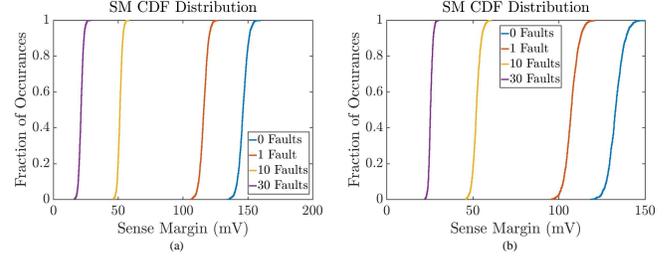

Fig. 10: Process variation analysis of SM for different number of failures on a single BL while bitcell consists of RRAM only at, (a) $-10°C$; (b) $90°C$.

RRAMs to the ground. Peripherals and the rest of the FTG's operation are the same as FTV.

2) Non-fixable Faults : Although FTV can fix most of the faults in a crossbar array, it is unable to handle some rare situations. For example, if there are two faulty BLs and the faulty RRAM on one of the BLs is the operand of the other BL. As shown in Fig. 8, BL_0 and BL_m are faulty and their operation must be done in the second cycle. In this case, the logic of BL_m gets lost if FTV forces input of the faulty RRAM ($RRAM1$) on BL_0 to V_{DD} since one of its inputs is set to V_{DD}. The $NAND$ operation for BL_m is incorrectly performed between in_n and '1' instead of between in_n and in_m. The probability of occurrence of such a fault for fabrication yields of more than 99% is less than 1%. We randomly distributed the faults for 100 times using $C++$ language rand function in order to achieve the percentage of faults occurring in an array.

3) Handling multiple faults: As long as faulty RRAMs in the crossbar array are independent of each other, FTV can handle as many as possible faults. For our simulations we inserted 30 faults in a 64*32 crossbar array and FTV was able to solve more than 99% of fault distribution over the array.

C. Finding Faults using FTV Peripherals

It is required to find the faulty RRAMs to set fault signals of the BLs and WLs. Faults can be found by the peripherals that are included in the FTV. However, the BLs must be tested one at a time. To find the faults in a $NAND$ array, input of each RRAM, which is set to LRS in a BL is forced to V_{DD} and the rest are forced to '0'. The output of the SA indicates whether a BL is faulty ('1') or fault-free ('0'). If the BL is faulty, we need to find out which RRAM is faulty on that BL. A divide-and-conquer approach cannot be used in this architecture since there might be more than one faulty RRAM per BL, so we use brute force algorithm to find faulty RRAM. The input of the RRAM-under-test is set to '0' while inputs of all other RRAMs are set to V_{DD}. If SA output is '0', the RRAM-under-test is deemed faulty and its flag is set to '1'. All faulty RRAMs can be found by repeating this operation for each RRAM in each BL sequentially.

D. Usage and Limitations of SATO/FTV/FTG

SATO/FTV/FTG should be enabled only when a fault has been detected in the test process. Therefore, the fault-free array will only incur area overhead but no performance loss. The faulty array will be salvaged at the cost of performance overhead. Note that SATO/FTV/FTG are only applicable to DCIM-based IMC. They cannot be applied to MAGIC or RRAM-based static IMC in the current form.

V. Simulation Results

To evaluate SATO and FTV, we compute performance metrics that include worst-case SM, BL-delay, average delay, average power, and energy consumption of a 64*32 DCIM RRAM crossbar array (VI). Based on the simulation results, FTV is more efficient than SATO.

A. SATO Simulation Results

Applying SATO to DCIM increases power and energy consumption by 12% and 127%, respectively (the worst case) and also performance is reduced by more than 50%. However,

TABLE VII: SATO power and energy consumption

# of Faults	0	1	3	5	10	15	20	30
Power (uW)	215.4	231.4	233	234	238	239	240	241.5
Energy (pJ)	4.3	9.4	9.4	9.5	9.6	9.7	9.7	9.8

SATO is able to handle ∼50% of the SA1 faults. SAs are very costly and occupy large area, which using SAs to shift data, increases power consumption and leads to higher energy consumption. Power and Energy consumption of SATO with different number of SA1 faults is reported in Table VII.

B. FTV/FTG Simulation Results

SM is the most important parameter when FTV is applied to DCIM. Increased number of LRS RRAMs connected to V_{DD} (ground) on a BL worsens the SM when '0' ('1') is the output. Considering $NAND-2$, the worst case '0' occurs when one of the operands is '0' and the other operand is '1'. In this case, there is a voltage division is between one LRS RRAM connected to '0' and one LRS RRAM which is connected to V_{DD}. When there is a faulty LRS RRAM on the BL and it is forced to V_{DD}, the worst case '0' is when two LRS RRAMs are connected to V_{DD} and one LRS RRAM is connected to '0' which lead to increased output '0' voltage on the BL. Increased BL voltage for the worst case '0' degrades the SM as shown in Fig. 11 (a).

The degradation in worst case SM happens when the bitcell is made of only a RRAM (i.e., no selector diode). However, DCIM employs a bidirectional diode in series with the RRAM. This series-connected bidirectional diode is included to reduce power consumption by dropping 0.5V across the 2 terminals. When the voltage difference between a BL and a WL is less then the selector diode threshold voltage there is no current between the BL and the WL. So, increased number of LRS inputs connected to V_{DD} (ground) does not affect the SM of DCIM (Fig. 11 (b)). The current of HRS RRAMs increases with temperature which results in higher sneak path currents. In an AND (OR) array, the higher sneak path currents pull up (down) BL voltage to degrade the SM. However, when number of faults increases, sneak paths currents become negligible compared LRS RRAMs which are connected to V_{DD} (ground). Simulation results (Fig. 11 (a)) show that the SMs in different temperatures become equal when the number of faults is more than 20.

Compared to the fault-free situation, FTV reduces power and energy consumption by >54% and >7% respectively (since, SAs consume a lot of power and in the case of FTV, SAs connected to faulty BLs are deactivate in the first cycle and SAs connected to fault-free BLs are deactivated in the second cycle). This is due to inactive BLs and SAs and a longer time of operation. However, the performance reduces by 50% due to two cycle operations. Average power and energy for the four consecutive AND operations in the 64*64 array are reported in Table VIII.
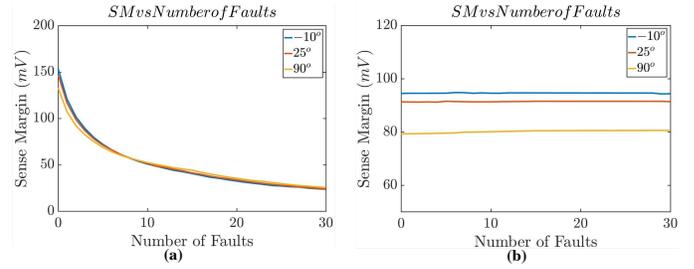

Fig. 11: SM for different number of faults in one BL at various temperatures, (a) diode+RRAM in the bitcell; (b) pure RRAM in the bitcell).

TABLE VIII: FTV power and energy consumption

# of Faults	0	1	3	5	10	15	20	30
Power (uW)	215.4	90	91.7	92.6	96.7	97.8	99	100.1
Energy (pJ)	4.3	3.6	3.7	3.7	3.9	3.9	4.0	4.0

C. Process Variation Simulations

The most important parameter to consider in a crossbar array under process variation is SM. We ran 1000-point MC simulations at $-10°C$, and $90°C$ on DCIM by considering the bitcell consisting of only a RRAM and RRAM and a selector diode with different number of SA1 faults. Simulation results for RRAM bitcell and RRAM and selector diode bitcell are shown in Fig. 9 and 10, respectively.

As shown in Fig. 9, variations do not affect SM significantly due to the presence of selector diode which stabilizes BL voltage. However, as demonstrated in Fig. 10, variations affect the SM when only RRAM is used in the crossbar. This is due to large changes in the RRAM resistance for a small change in RRAM gap when 1.2V is applied across it. Worst case SM with the number of failures for both w/ and w/o selector diode is reported in Table. IX.

VI. CONCLUSIONS

We proposed FAME for in-memory FP arithmetic computation. FAME implements single precision FP adder/subtractor using RRAM crossbar and evaluated two flavors with $NAND-NAND$ and $NOR-NOR$ compute arrays. We also proposed a novel SA based shift circuit for frequent shifting needed in FP operation. Compared to MAGIC-based implementation, FAME achieves 828X and 3.7X latency and energy improvement over MAGIC and compared to processing units (e.g. CPU, FPGA, GPU) it also reduces energy consumption and delay by 93% and 70%, respectively. FAME achieves lower power and energy consumption compared to MAGIC and processing units at low area overhead to the

TABLE IX: SM for different number of failures

Failures	SM (Selector diode)	SM (Without Selector Diode)
0	91.3 mV	118 mV
1	91.2 mV	95 mV
10	91.3 mV	44 mV
30	91.4 mV	19 mV

memory arrays. FAME uses 3KB memory to implement single precision FP operations (V). Furthermore, two approaches to mitigate HRS to LRS retention and stuck-at-1 failures in RRAM-based compute memories are proposed along with a test approach to identify faulty RRAMs. Forcing-to-V_{DD} (FTV) can mitigate 99% of the faults while reducing the power consumption by >50% and energy consumption by >7%. Shifting-at-the-Output (SATO) technique increases power consumption slightly but increases energy consumption by >50%.

REFERENCES

[1] Huangfu, W., Xia, L., Cheng, M., Yin, X., Tang, T., Li, B., Chakrabarty, K., Xie, Y., Wang, Y. and Yang, H., "Computation-oriented fault-tolerance schemes for rram computing systems," *22nd Asia and South Pacific Design Automation Conference (ASP-DAC)*, JAN 2017.

[2] Haj-Ali, A., Ben-Hur, R., Wald, N., Ronen, R. and Kvatinsky, S., "Imaging–in-memory algorithms for image processing," *IEEE Transactions on Circuits and Systems I: Regular Papers (TCAS1)*, JUN 2018.

[3] Linn, E., Rosezin, R., Tappertzhofen, S., Böttger, U. and Waser, R., "Beyond von neumann—logic operations in passive crossbar arrays alongside memory operations," *Nanotechnology*, JUL 2012.

[4] Agrawal, A., Jaiswal, A., Lee, C. and Roy, K., "X-sram: Enabling in-memory boolean computations in cmos static random access memories," *IEEE Transactions on Circuits and Systems I: Regular Papers (TCAS1)*, JUL 2018.

[5] Imani, M., Gupta, S. and Rosing, T., "Ultra-efficient processing in-memory for data intensive applications," *Proceedings of the 54th Annual Design Automation Conference 2017 (DAC 2017)*, JUN 2017.

[6] Zhang, J., Wang, Z. and Verma, N., "In-memory computation of a machine-learning classifier in a standard 6t sram array," *IEEE Journal of Solid-State Circuits (JSC)*, APR 2017.

[7] Motaman, S. and Ghosh, S., "Dynamic computing in memory (dcim) in resistive crossbar arrays," *ICCD*, OCT 2019.

[8] Kang, M., Keel, M.S., Shanbhag, N.R., Eilert, S. and Curewitz, K., "An energy-efficient vlsi architecture for pattern recognition via deep embedding of computation in sram," *IEEE International Conference on Acoustics, Speech and Signal Processing (ICASSP)*, pp. 8326–8330, MAY 2014.

[9] Patterson, D., Anderson, T., Cardwell, N., Fromm, R., Keeton, K., Kozyrakis, C., Thomas, R. and Yelick, K., "Intelligent ram (iram): Chips that remember and compute," *IEEE International Solids-State Circuits Conference. Digest of Technical Papers*, FEB 1997.

[10] Yin, X., Aziz, A., Nahas, J., Datta, S., Gupta, S., Niemier, M. and Hu, X.S., "Exploiting ferroelectric fets for low-power non-volatile logic-in-memory circuits," *IEEE/ACM International Conference on Computer-Aided Design (ICCAD)*, NOV 2016.

[11] Iyengar, A.S., Ghosh, S. and Jang, J.W., "Mtj-based state retentive flip-flop with enhanced-scan capability to sustain sudden power failure," *IEEE Transactions on Circuits and Systems I: Regular Papers*, vol. 62, no. 8, pp. 2062–2068, AUG 2015.

[12] Yin, X., Niemier, M. and Hu, X.S., "Design and benchmarking of ferroelectric fet based tcam," *Design, Automation & Test in Europe Conference & Exhibition (DATE)*, MAR 2017.

[13] Imani, M., Kim, Y. and Rosing, T, "Mpim: Multi-purpose in-memory processing using configurable resistive memory," *Asia and South Pacific Design Automation Conference (ASP-DAC)*, JAN 2017.

[14] Seshadri, V., Lee, D., Mullins, T., Hassan, H., Boroumand, A., Kim, J., Kozuch, M.A., Mutlu, O., Gibbons, P.B. and Mowry, T.C., "Buddy-ram: Improving the performance and efficiency of bulk bitwise operations using dram," *arXiv preprint arXiv:1611.09988*, 2016.

[15] Sayyah Ensan, S. and Ghosh, S., "Fpcas: In-memory floating point computations for autonomous systems," *The International Joint Conference on Neural Networks (IJCNN)*, JUL 2019.

[16] Kang, W., Wang, H., Wang, Z., Zhang, Y. and Zhao, W., "In-memory processing paradigm for bitwise logic operations in stt–mram," *IEEE Transactions on Magnetics*, vol. 53, no. 11, MAY 2017.

[17] Talati, N., Gupta, S., Mane, P. and Kvatinsky, S., "Logic design within memristive memories using memristor-aided logic (magic)," *IEEE Transactions on Nanotechnology*, vol. 15, no. 4, pp. 635–650, MAY 2016.

[18] Li, S., Xu, C., Zou, Q., Zhao, J., Lu, Y. and Xie, Y., "Pinatubo: A processing-in-memory architecture for bulk bitwise operations in emerging non-volatile memories," *ACM/EDAC/IEEE Design Automation Conference (DAC)*, JUN 2016.

[19] Li, B., Wang, Y., Chen, Y., Li, H.H. and Yang, H., "Ice: Inline calibration for memristor crossbar-based computing engine," *Design, Automation & Test in Europe Conference & Exhibition (DATE)*, MAR 2014.

[20] Xia, L., Gu, P., Li, B., Tang, T., Yin, X., Huangfu, W., Yu, S., Cao, Y., Wang, Y. and Yang, H, "Technological exploration of rram crossbar array for matrix-vector multiplication," *Journal of Computer Science and Technology*, JAN 2016.

[21] Xia, L., Huangfu, W., Tang, T., Yin, X., Chakrabarty, K., Xie, Y., Wang, Y. and Yang, H., "Stuck-at fault tolerance in rram computing systems," *IEEE Journal on Emerging and Selected Topics in Circuits and Systems*, MAR 2018.

[22] Zhang, B., Uysal, N., Fan, D. and Ewetz, R., "Handling stuck-at-faults in memristor crossbar arrays using matrix transformations," *Proceedings of the 24th Asia and South Pacific Design Automation Conference (ASPDAC)*, JAN 2019.

[23] Chen, C.Y., Shih, H.C., Wu, C.W., Lin, C.H., Chiu, P.F., Sheu, S.S. and Chen, F.T, "Rram defect modeling and failure analysis based on march test and a novel squeeze-search scheme," *IEEE Transactions on Computers*, JAN 2015.

[24] Kannan, S., Karimi, N., Karri, R. and Sinanoglu, O., "Detection, diagnosis, and repair of faults in memristor-based memories," *IEEE 32nd VLSI Test Symposium (VTS)*, APR 2014.

[25] B. Gao, H. Zhang, B. Chen, L. Liu, X. Liu, R. Han, J. Kang, Z. Fang, H. Yu, B. Yu *et al.*, "Modeling of retention failure behavior in bipolar oxide-based resistive switching memory," *IEEE Electron Device Letters*, vol. 32, no. 3, 2011.

[26] Kvatinsky, S., Belousov, D., Liman, S., Satat, G., Wald, N., Friedman, E.G., Kolodny, A. and Weiser, U.C., "Magic—memristor-aided logic," *IEEE Transactions on Circuits and Systems II: Express Briefs*, vol. 61, no. 11, pp. 895–899, SEP 2014.

[27] Patterson, D.A. and Hennessy, J.L., *Computer organization and design*. Morgan Kaufmann, 2007.

[28] Predictive technology model. [Online]. Available: http://ptm.asu.edu/

[29] Arizona state university rram model. [Online]. Available: http://nimo.asu.edu/memory/

[30] Huang, Jiun-Jia, Yi-Ming Tseng, Wun-Cheng Luo, Chung-Wei Hsu, and Tuo-Hung Hou., "One selector-one resistor (1s1r) crossbar array for high-density flexible memory applications," *Electron Devices Meeting (IEDM)*, 2011.

[31] Nho, H., Yoon, S.S., Wong, S.S. and Jung, S.O., "Numerical estimation of yield in sub-100-nm sram design using monte carlo simulation," *IEEE Transactions on Circuits and Systems II: Express Briefs*, 2008.

[32] Malladi et al, "Towards energy-proportional datacenter memory with mobile dram," *Annual International Symposium on Computer Architecture (ISCA)*, JUN 2012.